Spontaneous Four-Wave Mixing of de Broglie Waves: Beyond Optics

Valentina Krachmalnicoff, Jean-Christophe Jaskula, Marie Bonneau, Guthrie B. Partridge, Denis Boiron, Christoph I Westbrook, Piotr Deuar, Pawel Zin, Marek Trippenbach, Karen Kheruntsyan, et al.

Spontaneous Four-Wave Mixing of de Broglie Waves: Beyond Optics

V. Krachmalnicoff[1], J.-C. Jaskula[1], M. Bonneau[1], G. B. Partridge[1], D. Boiron[1], C. I. Westbrook[1], P. Deuar[2], P. Ziń[3], M. Trippenbach[4], and K.V. Kheruntsyan[5]

[1] *Laboratoire Charles Fabry de l'Institut d'Optique, Univ Paris Sud, CNRS, Campus Polytechnique RD128 91127 Palaiseau France*

[2] *Institute of Physics, Polish Academy of Sciences, Al. Lotników 32/46, 02-668 Warsaw, Poland*

[3] *The Andrzej Sołtan Institute for Nuclear Studies, Hoża 69, PL-00-681 Warsaw, Poland*

[4] *Institute of Theoretical Physics, Physics Department, University of Warsaw, Hoża 69, PL-00-681 Warsaw, Poland*

[5] *ARC Centre of Excellence for Quantum-Atom Optics, School of Mathematics and Physics, University of Queensland, Brisbane, Queensland 4072, Australia*

(Dated: November 24, 2009)

We investigate the atom-optical analog of degenerate four-wave mixing of photons by colliding two Bose-Einstein condensates (BECs) of metastable helium and measuring the resulting momentum distribution of the scattered atoms with a time and space resolved detector. For the case of photons, phase matching conditions completely define the final state of the system, and in the case of two colliding BECs, simple analogy implies a spherical momentum distribution of scattered atoms. We find, however, that the final momenta of the scattered atoms instead lie on an ellipsoid whose radii are smaller than the initial collision momentum. Numerical and analytical calculations agree well with the measurements, and reveal the interplay between many-body effects, mean-field interaction, and the anisotropy of the source condensate.

PACS numbers: 03.75.Nt, 34.50.-s, 05.30.-d,

The field of atom optics has developed to the point that one can now speak of the beginning of "quantum atom optics" [1] in which atoms are manipulated in ways similar to photons and in which quantum fluctuations and entanglement play an important role. The demonstration of atom pair production [2, 3], either from the dissociation of ultra-cold molecules, a process analogous to parametric down-conversion [4, 5, 6], or from collisions of BECs [7, 8, 9, 10], analogous to four-wave mixing (FWM) [11, 12, 13, 14, 15, 16, 17, 18, 19, 20, 21], holds considerable promise for generating atomic squeezed states and demonstrating nonlocal Einstein-Podolsky-Rosen (EPR) correlations [4, 5, 22, 23]. In both these systems, atom-atom interactions play the role of the nonlinear medium that allows conversion processes. Atoms are not, however, exactly like photons, and in spite of their formal similarity, the processes of pair production of photons and of atoms exhibit some interesting and even surprising differences that must be understood in order for the quantum atom optics field to advance. In this work, we discuss one such effect.

In optical FWM or parametric down conversion [24], energy conservation requires that the sum of the energies of the outgoing photons be fixed by the energy of the input photon(s). Phase matching requirements impose constraints on the directions and values of the individual photon momenta. A simple case is degenerate, spontaneous FWM (i.e. two input photons of equal energy) in an isotropic medium, for which energy conservation and phase matching require that the momenta of the output photons lie on a spherical shell whose radius is that of the momenta of the input photons.

We have performed the atom optical analog of degenerate FWM in colliding BECs while paying careful attention to the momenta of the outgoing atoms. We find that unlike the optical case, the output momenta do *not* lie on a sphere, but rather on an ellipsoid with short radius *smaller* than that of the input momenta. This behavior is due to a subtle combination of atom-atom interactions, which impose an energy cost for pair production, and the anisotropy of the condensates, which affects the evolution of the scattered atoms as they leave the interaction region. Although an analogous effect could exist in optics, optical nonlinearities are typically so small that the effect is rendered negligible and has therefore, to our knowledge, never been taken into account.

To fully understand the results, we have simulated the BEC collision using a fully quantum, first-principles numerical calculation based on the positive-P representation method [17, 20], and find quantitative agreement with the experiment. We have also analyzed the problem using a stochastic implementation of the Bogoliubov approach, which allows us to identify and illustrate the contributions of various interaction effects in the process.

The experimental setup is similar to that described in [3]. We start from a BEC of $\sim 10^5$ atoms magnetically trapped in the $m_x = 1$ sublevel of the 2^3S_1 metastable state of helium-4. The trap is cylindrically symmetric with axial and radial frequencies of 47 Hz and 1150 Hz, respectively. The bias field of ~ 0.25 G along the x-axis defines the quantization axis.

To generate the two colliding BECs, we use a two-step process. First, the atoms are transferred to the $m_x = 0$ state by a stimulated Raman transition. Using a 4 μs

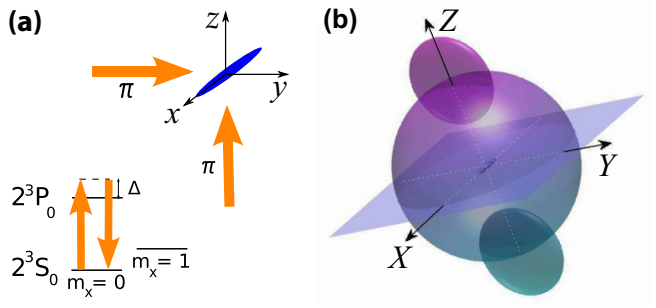

FIG. 1: (Color online) (a) Geometry of the Bragg beams and level scheme of the $2^3S_1 - 2^3P_0$ transition of ^{4}He (at 1083 nm). A Bragg pulse of two π-polarized laser beams (shown by the two arrows) detuned by $\Delta/2\pi = 600$ MHz produces two counterpropagating BECs that separate along their radial dimension at approximately 45° to the vertical (z) axis at relative velocity $2v_0$. (b) Schematic diagram of the collision geometry in the center-of-mass frame in which we denote the collision axis as Z. The two disks represent the colliding condensates in momentum space. The sphere represents the halo of scattered atoms. The cigar shaped initial condensate with axial direction $X = x$ is shown in the center. We analyze the experimental data in the XY-plane.

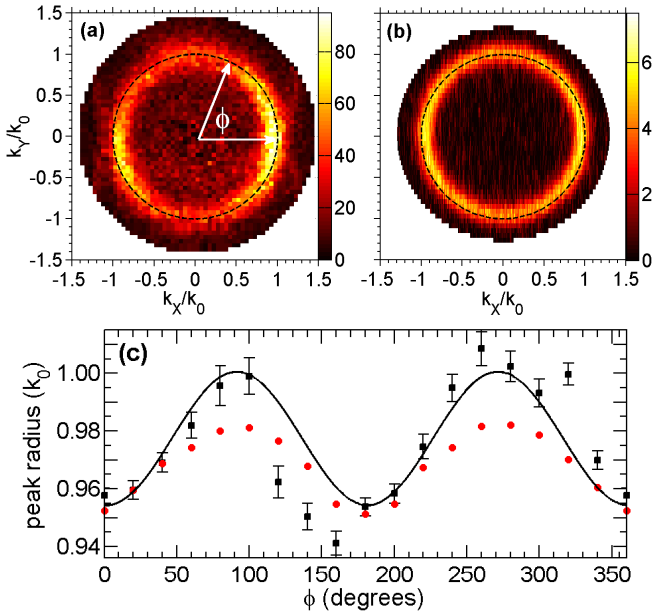

FIG. 2: (Color online) (a) Average momentum space density $n(k_X, k_Y)$ (in arb. units, from $\sim$ 1500 experimental runs) of the experimentally observed scattering halo on the equatorial plane (k_X, k_Y); the density is averaged over a disk of thickness $[-0.1k_0, +0.1k_0]$ along k_Z. (b) Same as in (a) but from the positive-P simulation (see text) after 70 μs collision time, in units of 10^{-18} m^3. (c) Plot of the peak radius of the scattering halo on the equatorial plane versus the azimuthal angle ϕ. Black squares are experimental data, while the red circles are from the simulation. The data is binned into 18 angular bins of $\Delta\phi = 20°$, and each data point for the peak radius is derived from a Gaussian fit to the radial distribution $n(k_R, \phi) \equiv n(k_X = k_R \cos\phi, k_Y = k_R \sin\phi)$ at the respective angle ϕ (the error bars show the statistical uncertainty in the fits; in addition, there is a systematic uncertainty of ±1.5% in the determination of the average radius of the sphere). The smooth line is a sinusoidal fit to the experimental data.

pulse duration, we transfer 90% of the atoms to this magnetically untrapped state. At a time 1 μs after the end of the Raman pulse, the BEC is split into two counterpropagating condensates with a Bragg pulse driven by two laser beams propagating at approximately 90°, as shown in Fig. 1 (a). The parameters of the Bragg pulse are adjusted to transfer half of the atoms to a state moving at relative velocity $2v_0$ in the yz-plane, with $v_0 = 7.31$ cm/s, which is ~ 4 times the speed of sound in the center of the BEC. The condensates thus separate along the *radial* axis, unlike in the experiment of Ref. [3]. To analyze the data we will use a center-of-mass reference frame, in which the collision axis is defined as Z (tilted by about 45° from z), $X \equiv x$, and Y is orthogonal to Z and X (see Fig. 1).

After the collision, the atoms fall onto a microchannel plate detector placed 46.5 cm below the trap center. A delay line anode permits reconstruction of a 3D image of the cloud of atoms. The flight time to the detector (300 ms), is long enough that the 3D reconstruction gives a 3D image of the velocity distribution after the collision. Binary, s-wave collisions between atoms in the BECs should (*naively*) result in the scattered particles being uniformly distributed on a sphere in velocity space with radius equal to the collision velocity v_0. The collision along the radial axis allows access to the entire collision halo in a plane containing the anisotropy of the BEC (the XY-plane) without distortion from the condensates. As in Ref. [3], we observe a strong correlation between atoms with opposite velocities confirming that the observed halo is indeed the result of binary collisions.

In Fig. 2 (a) we show a slice of the scattering halo in the XY-plane that reveals its annular structure. A dashed circle of radius 1, indicating the momentum $\hbar k_0 = mv_0$, is shown for comparison. We can see that the ring corresponding to the mean momentum of scattered atoms does not lie exactly on the dashed line, but rather slightly within it, and that the deviation is anisotropic. The thickness and density of the ring are also anisotropic, though in the present work we concentrate on the behavior of the radius [25]. To analyze the data more quantitatively, we divide the ring into azimuthal sectors and fit a Gaussian peak plus a linearly sloped background to extract a value for the halo radius as a function of the angle ϕ [20]. It is clear from Fig. 2 (c) that the radius of the halo in momentum space varies approximately sinusoidally by ±2% and that it is almost always smaller than k_0.

To understand this result qualitatively, we first con-

sider the energy balance for pair production in a homogeneous BEC. Removing an atom from the condensate liberates an energy corresponding to the chemical potential, $g\rho$, where $g = 4\pi a\hbar^2/m$, a is the s-wave scattering length, and ρ the density. Here, we have two counterpropagating condensates (each having density $\rho/2$), which for simplicity we model as plane waves. In the presence of the spatial modulation due to their interference, the energy liberated by removing one atom changes to $3g\rho/2$ [26]. On the other hand, placing an atom in a scattering mode requires an energy $2g\rho$ since the scattered atom is distinguishable from those in the condensate. Energy conservation, including the mean-field contributions, gives

$$\frac{\hbar^2 k_0^2}{2m} + \frac{3}{2}g\rho = \frac{\hbar^2 k_s^2}{2m} + 2g\rho, \tag{1}$$

where we denote the absolute momentum of one scattered atom $\hbar k_s$. Thus, the scattered momentum is *smaller* than the ingoing momentum, $k_s < k_0$. This effect was observed in a numerical simulation in Ref. [14]; a similar effect was discussed in Ref. [8]. Using plane waves to model the BECs is of course a crude approximation, but if we replace ρ by the central density of an inhomogeneous BEC, we find $k_s = 0.96\,k_0$ for the experimental parameters.

In addition to this initial energy balance analysis, a second effect must be taken into account. Once created, the scattered atoms escape from the condensate region and gain energy from the mean-field interaction potential. The effect is similar to that reported in Ref. [26], an experiment which observed the mutual repulsion of two BECs after Bragg diffraction. In our system, the potential also evolves in time and goes to zero in the XY-plane on a timescale corresponding to the time for the two condensates to separate (~ 70 μs). The rapid vanishing of the potential on the equatorial plane has a very different effect on scattered atoms moving in the X and Y directions. Atoms moving along Y, the small dimension of the trap, escape the condensate overlap region on a timescale of ~ 40 μs, faster than the condensates can separate. As a result, these atoms are substantially accelerated by a steep potential gradient. On the other hand atoms moving along X, the long axis of the trap, do not escape before the condensates separate and thus experience much less acceleration. Accordingly the observed momentum along the X direction is smaller than along Y, and much closer to the shifted value predicted by Eq. (1).

To describe this experiment quantitatively we perform first-principles positive-P simulations similar to those in Refs. [17, 20]. Here, the multimode dynamics of the atomic field operators $\hat{\Psi}(\mathbf{x},t)$ and $\hat{\Psi}^\dagger(\mathbf{x},t)$ for the $m_x = 0$ state is fully modeled by two independent complex c-fields, $\Psi(\mathbf{x},t)$ and $\tilde{\Psi}(\mathbf{x},t)$, satisfying the Îto stochastic differential equations:

$$\begin{aligned} i\hbar\partial_t\Psi(\mathbf{x},t) &= \mathcal{A}_{\rm GP}(\Psi,\tilde{\Psi})\Psi + \sqrt{i\hbar g}\Psi\zeta_1(\mathbf{x},t), \\ -i\hbar\partial_t\tilde{\Psi}(\mathbf{x},t) &= \mathcal{A}_{\rm GP}(\Psi,\tilde{\Psi})\tilde{\Psi} + \sqrt{-i\hbar g}\tilde{\Psi}\zeta_2(\mathbf{x},t). \end{aligned} \tag{2}$$

Here, $\mathcal{A}_{\rm GP}(\Psi,\tilde{\Psi}) = -\hbar^2\nabla^2/(2m) + g\tilde{\Psi}\Psi$ is a deterministic part similar to the mean-field Gross-Pitaevskii (GP) equation, $\zeta_j(\mathbf{x},t)$ ($j = 1,2$) are real independent noise sources with zero mean and correlations $\langle\zeta_j(\mathbf{x},t)\zeta_k(\mathbf{x}',t')\rangle = \delta_{jk}\delta^{(3)}(\mathbf{x}-\mathbf{x}')\delta(t-t')$, while $g = 4\pi\hbar^2 a/m$ uses $a = 5.3$ nm [3] for the $m_x = 0$ atoms.

The initial condition is a coherent state with the density profile $\rho(\mathbf{x})$ of the initially trapped $m_x = 1$ state BEC with $a = 7.51$ nm [27], $N_0 = 10^5$ atoms, and modulated with a standing wave that imparts initial momenta $\pm k_0$ in the Z direction,

$$\Psi(\mathbf{x},0) = \langle\hat{\Psi}(\mathbf{x},0)\rangle = \sqrt{\rho(\mathbf{x})/2}\left(e^{ik_0 \mathrm{Z}} + e^{-ik_0 \mathrm{Z}}\right). \tag{3}$$

This models a Bragg pulse at $t = 0$ that splits the BEC into two equal halves, described in the center-of-mass frame. The initial density $\rho(\mathbf{x})$ is obtained as the ground state solution to the GP equation in the trap, and $\tilde{\Psi}(\mathbf{x},0) = \Psi(\mathbf{x},0)^*$. The results of this simulation are shown in Fig. 2 (b) and (c) for $t = 70$ μs at which time the condensates have fully separated and the collision is over. The result of the simulation is in very good agrement with the experiment. The small discrepancy between the experimental data and the simulation in the anisotropy of the peak radius could be because the experiment, unlike the simulation, averages over a broad distribution of initial atom numbers. Since large condensates scatter more atoms, this fact may bias the experimental data towards larger modulations.

In order to confirm the qualitative mean-field mechanisms described above, we also perform an analysis of the collision dynamics using a time-adaptive Bogoliubov approach [28], in which the atomic field operator is split into the mean-field (ψ_0) and fluctuating components, $\hat{\Psi}(\mathbf{x},t) = \psi_0(\mathbf{x},t) + \hat{\delta}(\mathbf{x},t)$. The coherent BEC wavefunction $\psi_0(\mathbf{x},t)$ evolves according to the standard time-dependent GP equation, with the initial condition given by Eq. (3). The fluctuating component $\hat{\delta}(\mathbf{x},t)$ describes incoherent scattered atoms, and is initially in the vacuum state. In the Bogoliubov approach, $\hat{\delta}$ evolves as

$$i\hbar\partial_t\hat{\delta}(\mathbf{x},t) = \mathcal{H}_0(\mathbf{x},t)\hat{\delta} + \mathcal{G}(\mathbf{x},t)\hat{\delta}^\dagger. \tag{4}$$

Here, $\mathcal{H}_0(\mathbf{x},t) = -\hbar^2\nabla^2/(2m) + 2g|\psi_0(\mathbf{x},t)|^2$ contains the kinetic energy and the mean-field potential energy $2g|\psi_0(\mathbf{x},t)|^2$ for scattered atoms. The effective coupling $\mathcal{G}(\mathbf{x},t) = g\,\psi_0(\mathbf{x},t)^2$ causes spontaneous pair production of scattered atoms. The dynamics of the field $\hat{\delta}$ is then formulated using the positive-P representation [28], leading to the (stochastic field) evolution equations

$$\begin{aligned} i\hbar\partial_t\delta(\mathbf{x},t) &= \mathcal{H}_0\delta + \mathcal{G}\tilde{\delta} + \sqrt{i\mathcal{G}}\zeta_1(\mathbf{x},t), \\ -i\hbar\partial_t\tilde{\delta}(\mathbf{x},t) &= \mathcal{H}_0\tilde{\delta} + \mathcal{G}^*\delta + \sqrt{-i\mathcal{G}^*}\zeta_2(\mathbf{x},t). \end{aligned} \tag{5}$$

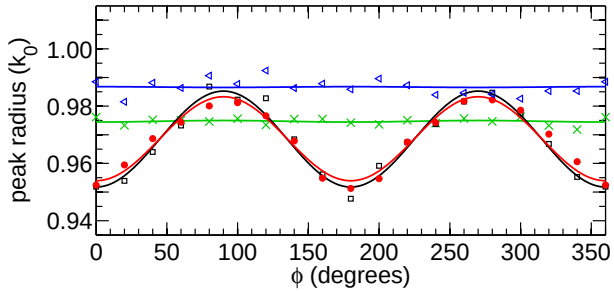

FIG. 3: (Color online) Predictions for the radius of the scattering halo as in Fig. 2 (c) with various controlled changes. *Red*–•: full positive-P calculation, Eq. (2) [same data as in Fig. 2 (c)]; *Black*–□: full anisotropic Bogoliubov calculation, Eq. (5); *Blue*–◁: anisotropic Bogoliubov, but with mean-field potentials $\propto g|\psi_0|^2$ removed from Eq. (5) and from the GP equation describing the evolution of $\psi_0(\mathbf{x},t)$; *Green*–×: full Bogoliubov, but with *spherical* BECs and unchanged peak density $\rho(0)$. Data was obtained from Gaussian fits to the radial densities $n(k_R,\phi)$ in the XY plane after the end of the collision at 72 μs (200 μs for the spherical case).

which, unlike the full calculation (2), are stable in time because the noise is non-multiplicative. This method takes into account the temporal evolution and spatial separation of the two condensates; the stochastic formulation of the evolution of the field $\hat{\delta}(\mathbf{x},t)$ makes explicit diagonalizations on the (enormous) Hilbert space unnecessary. As condensate depletion is $\sim 1.5\%$ here, the stochastic Bogoliubov results are in excellent agreement with the positive-P simulations, as seen in Fig. 3.

Figure 3 also shows simulations performed with controlled changes applied to the system. They directly confirm that: (1) The mean-field potential is essential for both appreciable radius shift and ellipticity (*Blue*–◁ data correspond to simulations without any mean-field potential); (2) Anisotropy of the initial BEC is essential for ellipticity in the XY-plane (*Green*–× data had an initially spherical condensate and shows no ellipticity). The fact that the blue data shows $k_s/k_0 \simeq 0.987$ and not unity is expected. The prediction of unity comes from energy conservation. The simulation data does indeed lie on the line $k_s/k_0 = 1$ if one extracts the peak radius k_s from the *energy* density $\propto k_R^2 n(k_R,\phi)$, rather than from $n(k_R,\phi)$ as in the figure.

In summary, the ability to detect three dimensional momentum vectors of individual atoms allows the identification of small, previously unseen anomalies in the scattering "sphere" resulting from a simple collision between two condensates. First-principles simulations closely reproduce for these small anomalies and help us to identify the important physical processes. Our results highlight the complexities of atomic scattering that must be accounted for in future applications of ultracold atoms in precision measurement and fundamental tests using squeezed [29, 30] and entangled [31] atomic ensembles.

This work was supported by the French ANR, the IFRAF institute, and the Euroquam Project CIGMA. GP is supported by the European Union Marie Curie IIF Fellowship no. 220264. PD acknowledges the European Union contract MEIF-CT-2006-041390. PZ and MT are supported by Polish Government Research Grants. KK acknowledges support by the Australian Research Council through the ARC Centre of Excellence scheme, and the hospitality of the Université Paris-Sud 11.

[1] P. Meystre, *Atom Optics* (Springer, Berlin, 2001).
[2] M. Greiner *et al.*, Phys. Rev. Lett. **94**, 110401 (2005).
[3] A. Perrin *et al.*, Phys. Rev. Lett. **99**, 150405 (2007).
[4] T. Opatrný and G. Kurizki, Phys. Rev. Lett. **86**, 3180 (2001).
[5] K. V. Kheruntsyan and P. D. Drummond, Phys. Rev. A **66**, 031602(R) (2002).
[6] C. M. Savage, P. E. Schwenn, and K. V. Kheruntsyan, Phys. Rev. A **74**, 033620 (2006).
[7] L. Deng *et al.*, Nature **398**, 218 (1999).
[8] J. M. Vogels, K. Xu, and W. Ketterle, Phys. Rev. Lett. **89**, 020401 (2002).
[9] J. M. Vogels, J. K. Chin, and W. Ketterle, Phys. Rev. Lett. **90**, 030403 (2003).
[10] N. Katz *et al.*, Phys. Rev. A **70**, 033615 (2004).
[11] H. Pu and P. Meystre, Phys. Rev. Lett. **85**, 3987 (2000).
[12] L.-M. Duan, A. Sørensen, J. I. Cirac, and P. Zoller, Phys. Rev. Lett. **85**, 3991 (2000).
[13] Y. B. Band, M. Trippenbach, J. P. Burke, and P. S. Julienne, Phys. Rev. Lett. **84**, 5462 (2000).
[14] R. Bach, M. Trippenbach, and K. Rzążewski, Phys. Rev. A **65**, 063605 (2002).
[15] P. Ziń *et al.*, Phys. Rev. Lett. **94**, 200401 (2005).
[16] A. A. Norrie, R. J. Ballagh, and C. W. Gardiner, Phys. Rev. Lett. **94**, 040401 (2005).
[17] P. Deuar and P. D. Drummond, Phys. Rev. Lett. **98**, 120402 (2007).
[18] K. Mølmer *et al.*, Phys. Rev. A **77**, 033601 (2008).
[19] J. Chwedeńczuk *et al.*, Phys. Rev. A **78**, 053605 (2008).
[20] A. Perrin *et al.*, New J. Physics **10**, 045021 (2008).
[21] M. Ögren and K. V. Kheruntsyan, Phys. Rev. A **79**, 021606(R) (2009).
[22] K. V. Kheruntsyan, M. K. Olsen, and P. D. Drummond, Phys. Rev. Lett. **95**, 150405 (2005).
[23] A. J. Ferris, M. K. Olsen, and M. J. Davis, Phys. Rev. A **79** 043634 (2009).
[24] M. O. Scully and M. S. Zubairy, *Quantum Optics* (Cambridge University Press, Cambridge, UK, 1997).
[25] J.-C. Jaskula *et al.*, in preparation.
[26] J. Simsarian *et al.*, Phys. Rev. Lett. **85**, 2040 (2000).
[27] S. Moal *et al.,* Phys. Rev. Lett. **96**, 023203 (2006).
[28] P. Deuar *et al.*, in preparation.
[29] C. Orzel *et al.*, Science **291**, 2386 (2001).
[30] C.-S. Chuu *et al.* Phys. Rev. Lett. **95**, 260403 (2005).
[31] J. Estève *et al.*, Nature (London) **455**, 1216 (2008).